Hydrogen Storage

DOI: 10.1002/ange.201206055

Magnesium Nanocrystals Embedded in a Metal–Organic Framework: Hybrid Hydrogen Storage with Synergistic Effect on Physi- and Chemisorption**

*Dae-Woon Lim, Ji Woong Yoon, Keun Yong Ryu, and Myunghyun Paik Suh**

Hydrogen is considered to be a promising energy carrier for the future. In order to use it as a fuel, a compact, safe, and efficient hydrogen storage system should be developed. Porous metal–organic frameworks (MOFs) have attracted great attention as potential hydrogen storage materials,[1] because some MOFs can store large amount of H_2 (>7 wt%) at 77 K and high pressures.[2] However, at room temperature, the H_2 storage capacities of MOFs drop to less than 1 wt% because interaction energies between the frameworks and H_2 are very low (4–8 kJ mol^{-1}). There have been efforts to enhance the H_2 storage capacities of MOFs at ambient temperature by methods such as tuning the ligand,[3] generation of open metal sites,[4] and embedding palladium nanoparticles.[5] Despite these modifications, the improvements were not very satisfactory, and none of the materials have yet met the target of the US Department of Energy (DOE) of 2017.

In search for a highly efficient material for H_2 storage, we have investigated the possibilities of hybrid materials that would be capable of storing H_2 by both physical adsorption and chemisorption. In particular, we have been interested in composite materials that consist of a MOF and magnesium nanoparticles. Magnesium chemisorbs H_2 at 773 K and 200 atm in the presence of MgI_2 catalyst.[6] Magnesium powder of 50–100 μm size made by ball milling slowly absorbs H_2 at 673 K and 10 bar.[7] The resulting magnesium hydride has a quite high dehydrogenation enthalpy ($\approx$75 kJ per mol H_2),[8] and therefore heavy-metal catalysts should be used to reduce the H_2 desorption temperature and improve kinetics, but they still do not allow effective dehydrogenation.[9] In the presence of heavy-metal catalysts, the H_2 absorption and release temperatures decrease as a result of destabilization of the metal hydride when the particle size of magnesium is reduced.[10]

Nanosized magnesium particles have been synthesized by a variety of methods, such as ball-milling,[11] condensation of magnesium metal vapor,[12] plasma metal reaction,[13] infiltration of melted Mg in carbon material,[14] and sonoelectrochemistry[15] or chemical reduction of Mg precursors.[16] Some of the disadvantages of these methods are that they require a long process time, extremely high temperatures (898–1203 K), and electrically or chemically harsh conditions, and yet they provide inhomogeneous size distributions.

Herein we report a simple method for fabrication of hexagonal-disk-shaped magnesium nanocrystals (Mg NCs) within a MOF. The fabrication of Mg nanocrystals inside MOFs is unprecedented. Previously, small Ag, Au, Ni, Pd, Ru, or Pt nanoparticles (size, 1.4–10 nm) were prepared in MOFs by immersing redox-active MOFs in the metal-ion solutions[5,17] or by reducing the metal precursors deposited in the MOFs.[18] The present nanocomposite is made by the thermal decomposition of air-sensitive bis-cyclopentadienyl magnesium ($MgCp_2$) vapor in a MOF, leading to the deposition of MG NCs in the MOF, a method that is also unprecedented for production of nanosized Mg. The resulting Mg NCs@MOF is a hybrid hydrogen storage material that stores H_2 by both physical adsorption and chemisorption, exhibiting a synergistic effect to increase the isosteric heat of H_2 physisorption and decrease the temperatures for chemisorption/desorption of H_2.

Yellow crystals of $[Zn_4O(atb)_2]\cdot 22\,DMF\cdot 9\,H_2O$ (SNU-90), in which atb is aniline-2,4,6-tribenzoate, were synthesized by heating a mixture of $Zn(NO_3)_2$ and H_3(atb) in dimethylformamide (DMF). The X-ray single-crystal structure of SNU-90 indicated a non-interpenetrated (6,3)-connected net of a *qom* topology, similar to MOF-177[19] (see the Supporting Information, Figures S1 and S2). When the guest solvent molecules in SNU-90 were removed by treatment with supercritical CO_2,[2b,20] a guest-free $[Zn_4O(atb)_2]$ (SNU-90′, NH_2-MOF-177) was obtained.

Vapor of bis(cyclopentadienyl) magnesium ($MgCp_2$) was deposited in SNU-90′ at 80 °C, and the resulting $MgCp_2$@SNU-90′ was thermally decomposed at 200 °C under an argon atmosphere followed by evacuation, which gave rise to Mg NCs embedded in SNU-90′. Thus far it was unknown that the thermal decomposition of $MgCp_2$ results in

[*] D.-W. Lim, Prof. M. P. Suh
Department of Chemistry, Seoul National University
Seoul 151-747 (Republic of Korea)
E-mail: mpsuh@snu.ac.kr
Dr. J. W. Yoon
Catalysis Center for Molecular Engineering
Korea Research Institute of Chemical Technology (KRICT)
Jang-dong 100, Yuseong, Deajeon 305-600 (Republic of Korea)
K. Y. Ryu
Division of Electron Microscopic Research
Korea Basic Science Institute
113 Gwahangno, Daejeon 305-333 (Korea)

[**] This work was supported by the National Research Foundation of Korea (NRF) Grant funded by the Korean Government (MEST) (No. 2011-0031432 and No. 2012-0000651). D.-W. Lim acknowledges support by Hi Seoul Science Fellowship from Seoul Scholarship Foundation. We thank Dr. H. S. Jung in Korea Basic Science Institute for helping us to perform electron microscopy work.

Supporting information for this article is available on the WWW under http://dx.doi.org/10.1002/anie.201206055.

Table 1: N_2 and H_2 gas uptake data in SNU-90′ and various samples of Mg@SNU-90′.

Compound	mol_{Mg}/mol_{Zn} (wt%)	N_2 uptake [$cm^3 g^{-1}$]	Surface area [$m^2 g^{-1}$]		Pore volume [$cm^{-3} g^{-1}$]	H_2 uptake [wt%] at 1 atm	at high pressure	Q_{st} [kJ mol^{-1}]
SNU-90′	n.a.	1135	4244[a]	4914[b]	1.64[c]	1.21 (77 K) 0.74 (87 K)	8.81 (77 K, 75 bar) 0.45 (298 K, 80 bar)	4.55
Mg@SNU-90′a	0.15 (1.26)	1104	4154[a]	4757[b]	1.47[c]	1.24 (77 K) 0.65 (87 K)	8.74 (77 K, 89 bar) 0.54 (298 K, 90 bar)	5.68
Mg@SNU-90′b	0.85 (6.52)	559	2056[a]	2373[b]	0.84[c]	0.72 (77 K) 0.40 (87 K)	0.29 (473 K, 30 bar)	7.24
Mg@SNU-90′c	1.40 (10.5)	378	1371[a]	1581[b]	0.36[c]	0.60 (77 K) 0.47 (87 K)	0.20 (323 K, 80 bar) 0.24 (415 K, 40 bar) 0.71 (473 K, 30 bar)	11.6

[a] BET surface area. [b] Langmuir surface area, and [c] Pore volume estimated by using the Dubinin–Radushkevich (DR) equation. n.a. = not available.

nanosized Mg, although it was reported that reduction of $MgCp_2$ with Li^+(naphthalenide$^-$) in a solution of polymethylmethacryate in tetrahydrofuran afforded round-shaped Mg nanoparticles.[16] As for the mechanism of the thermal decomposition, formation of metal and two C_5H_5 radicals that might further dissociate or associate to the complex products, was predicted as an initial step based on the theoretical calculation.[21] However, in order to verify the mechanism in our case, further research should be carried out. By changing the reaction conditions during the deposition process of $MgCp_2$, such as the duration time and whether or not a prevacuum state was applied to the reaction vessel, we could control the loaded amounts of $MgCp_2$ in the MOF and obtained several samples embedded with different amounts of magnesium nanocrystals (Supporting Information, Table S1).

The samples, Mg@SNU-90′a, Mg@SNU-90′b, and Mg@SNU-90′c, were loaded with 1.26 wt%, 6.52 wt%, and 10.5 wt% of Mg NCs, respectively, as determined by inductively coupled plasma atomic emission spectroscopy (ICP-AES) (Table 1). The NMR spectra indicated the absence of cyclopentadiene (Cp) in the resulting nanocomposites (Supporting Information, Figure S3).

The HRTEM images for various samples of Mg@SNU-90′ showed hexagonal-disk-shaped magnesium nanocrystals,[22] which have a diagonal length of hexagon ranging 44–88 nm (average (60 ± 18) nm) with a thickness ranging 16–61 nm (average (37 ± 12) nm; see Figure 1 and Figure S4 in the Supporting Information). Although it was reported that hexagonal-disk-shaped Mg NCs could be formed when Mg powder was heated at temperatures higher than 500°C,[22b] in the present work, they are formed by heating $Mg(Cp)_2$@MOF at only 200°C. The formation of Mg NCs that are much bigger than the channel size (12.9 Å × 9.6 Å) of the MOF is attributed to the agglomerization of nanoparticles by heat during the thermal decomposition. Alternatively, it is simply caused by the degradation of the MOF under electron-beam irradiation during the observation by HRTEM.[23] The selected-area electron diffraction (SAED) patterns of Mg NCs embedded in SNU-90' showed lattice fringes separated by 2.7871 Å, which is in agreement with the (100) *d*-spacing of metallic Mg (2.7782 Å, JCPDS 04-0770). The size distribution of the Mg NCs was found to be very similar in all of the samples, even though there were significantly different amounts of Mg NCs embedded in the MOF. When Mg@SNU-90′ was exposed to air for three weeks, the shape of the Mg NCs changed to a star shape that has a lattice fringe with a separation of 2.1101 Å, which corresponds to the (200) *d*-spacing of MgO (2.1061 Å, JCPDS 89-7746; Supporting Information, Figure S4). XPS data of Mg@SNU-90′ indicated that Mg^0 and Zn^{II} coexisted in the solid (Supporting Information, Figure S5).

To verify that the Mg NCs were embedded inside the channels of the MOF, we performed electron tomography. From the TEM images that were collected with a 1° interval with the tilting angle of +40°–−40°, 3D images were constructed by using the IMOD program.[24] When the sample was tilted, the shape of a Mg NC changed from hexagon to rectangle and from rectangle to hexagon, thus indicating that the Mg NCs were indeed embedded in the MOF (Figure 2 and Supporting Video).

The powder X-ray diffraction (PXRD) patterns showed that the structure of SNU-90' was maintained even after the formation of Mg NCs, the sizes of which were much larger than the channel size (12.9 Å × 9.6 Å) of the MOF (Supporting Information, Figure S6). To understand this observation,

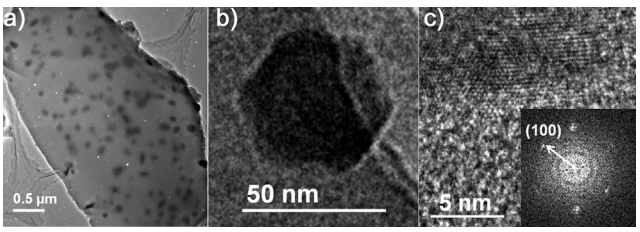

Figure 1. High-resolution transmission electron microscopy (HRTEM) images. a) Mg@SNU-90′b. b) A hexagonal-shaped Mg nanocrystal and c) its edge image showing lattice fringes with a separation of 2.7871 Å, which corresponds to (100) *d*-spacing of Mg^0 (2.7782 Å, JCPDS 04-0770). Inset: selected-area electron diffraction (SAED) pattern.

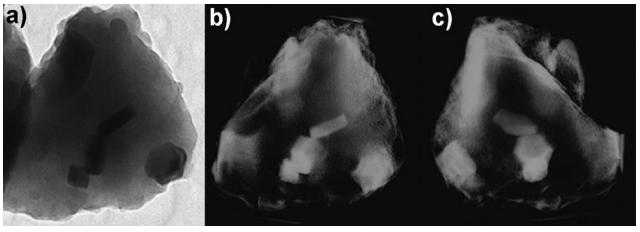

Figure 2. TEM and electron tomography images of Mg@SNU-90′b. a) TEM image. b) and c) Tomographically reconstructed images of Mg NCs embedded in SNU-90′ at different angles.

we calculated the ratio of the volumes of formed Mg NCs and the network skeleton for Mg@SNU-90′c. Assuming that all Mg NCs destroyed the network skeleton, the Mg NCs would destroy a maximum 4.6 % of the network skeleton by volume. This value is too small to alter the PXRD pattern of the MOF. It was also previously reported that metal nanoparticles much bigger than the cavity sizes of the hosts were impregnated by maintaining the network structures.[5,17] The PXRD peaks of crystalline Mg should generally appear at $2\theta = 32.2$, 34.4, and 36.6°, but we could observe only a peak at 36.6°, which is the strongest peak of Mg (Figure S7). On exposure to air for two days, however, the PXRD pattern showed the peaks corresponding to MgO, with retention of the framework structure of SNU-90′.

The adsorption–desorption isotherms were measured for N_2 gas at 77 K and for H_2 gas at various temperatures on SNU-90′, Mg@SNU-90′a, Mg@SNU-90′b, and Mg@SNU-90′c (Figure 3 Table 1). The N_2 gas sorption isotherms of the four samples were of type I, which is characteristic for the microporous materials (Supporting Information, Figure S8.). Despite the presence of the NH_2 group in the ligand of SNU-90′, the surface area, pore volume, and H_2 adsorption capacities of SNU-90′ were similar to those of MOF-177.[19] Gas sorption data for various samples of Mg@SNU-90′ showed that as the amount of Mg increased, the BET surface area, pore volume, and H_2 uptake capacity at 77 K and 1 atm decreased, because Mg NCs occupied the surface and space of the pores in the MOF. At 298 K and high pressure, however, the H_2 uptake in Mg@SNU-90′a increased by 20 %, to 0.54 wt % from 0.45 wt % in pristine SNU-90′, thus suggesting that Mg NCs provide a positive effect on H_2 adsorption at 298 K (Supporting Information, Figure S9). The zero-coverage isosteric heats of the H_2 adsorption, which were estimated from the H_2 adsorption isotherms measured at 77 K and 87 K, increased as the amount of Mg increased, up to 11.6 kJ mol^{-1} for Mg@SNU-90′c from 4.55 kJ mol^{-1} for SNU-90′ (Table 1, Figure 3).

In order to observe the chemisorption ability of the embedded Mg NCs, we also measured the H_2 uptake in Mg@SNU-90′c at 323 K, 415 K, and 473 K under high pressures (Figure 4). Contrary to the physisorbed MOFs, in which H_2 uptake decreases at the elevated temperature, the H_2 chemisorption capacities of the present material increase as the temperature is raised. The H_2 absorption capacities of Mg@SNU-90′c were 0.20 wt % at 323 K under the H_2 pressure of 80 bar, 0.24 wt % at 415 K under the H_2 pressure of 40 bar. At 473 K under 30 bar, the H_2 uptake capacity of Mg@SNU-90′c became 0.71 wt % (volumetric H_2 storage capacity, 3.1 g L^{-1}). This value is remarkably higher than that of Mg@SNU-90′b under the same conditions (Table 1), despite the former exhibiting a much lower surface area and pore volume because of the heavily loaded Mg. The fact that the H_2 uptake enhances with elevated temperatures and the increased amount of Mg NCs confirms that the H_2 uptakes in Mg@SNU-90′ at 323 K, 415 K, and 473 K are results of chemisorption. These chemisorption temperatures are significantly lower (by > 200 K) than that (673 K under 10 bar) of bare Mg powder of 50–100 μm in size.[7] If the H_2 uptake capacity of Mg alone is estimated from the data, it is 7.5 wt % at 473 K and 30 bar. Considering that the H_2 chemisorption capacity of pure Mg is 7.66 wt %, 99 % of the Mg NCs in the sample chemisorb H_2, which is much better than any form of Mg previously reported, such as Mg nanoparticles incorporated in a polymer[16] and bare Mg powder.[25]

The H_2 desorption properties of Mg@SNU-90′c were verified by the temperature-programmed desorption mass spectroscopy (TPD-MS) analysis (Figure 4 d). The TPD-MS results indicated that H_2 was desorbed at $T > 523$ K and 1 atm. It should be noted that the signal intensities of hydrogen atoms were exactly twice as strong as those of H_2 molecules (Supporting Information, Figure S10). This observation sug-

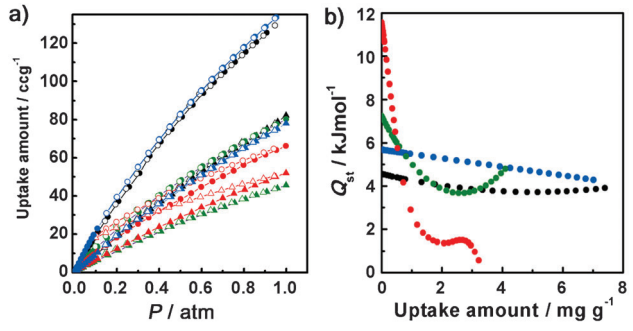

Figure 3. Physical adsorptions of H_2 in SNU-90′ (black), Mg@SNU-90′a (blue), Mg@SNU-90′b (green), and Mg@SNU-90′c (red). a) The H_2 adsorption isotherms at 77 K (circles) and 87 K (triangles). Filled shape: adsorption, open shape: desorption. b) Isosteric heats of the H_2 adsorption. The samples of Mg@SNU-90′a, Mg@SNU-90′b, and Mg@SNU-90′c contain 1.26 wt %, 6.52 wt %, and 10.5 wt %, respectively, of magnesium nanocrystals.

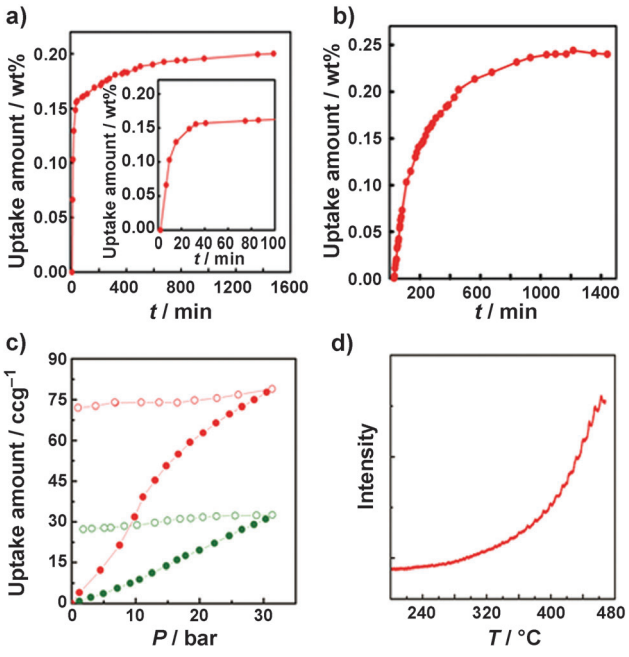

Figure 4. Chemical absorption of H_2 in Mg@SNU-90′c. a) H_2 absorption kinetics at 325 K and 80 bar. Inset: data with a magnified time scale. b) H_2 absorption kinetics at 415 K and 40 bar. c) H_2 absorption isotherms at 473 K in Mg@SNU-90′b (green) and Mg@SNU-90′c (red). Filled shapes: adsorption; open shapes: desorption. d) Temperature programmed desorption mass spectroscopy (TPD-MS) data; $m/e = 2$, measured under argon.

gests that all desorbed H_2 sources were MgH_2 not from the MOF at all. The TG mass loss of Mg@SNU-90′c after H_2 absorption is also in good agreement with the TPD-MS data (Supporting Information, Figure S11).

After the H_2 chemisorption at 473 K and 30 bar, the HRTEM images of Mg@SNU-90′c indicated that the crystal morphology of Mg was maintained but the crystal size was remarkably increased. The SAED pattern indicated the lattice fringe with a separation of 2.247 Å, which is in good agreement with the (110) *d*-spacing of β-MgH_2 (2.257 Å, JCPDS 35-1185, Supporting Information, Figure S12). The MgH_2@SNU-90′ shows the crystal size (diagonal length of hexagon) of average (142 ± 41) nm and thickness of average (83 ± 18) nm (Supporting Information, Figure S12), circa 2.3 times as large as those of Mg NCs. Considering that the volume of Mg should be increased by 30% on hydride formation,[26] this excessive expansion during the H_2 chemisorption processes at high temperature and pressure can be explained by the three-dimensional Ostwald ripening, in which the larger crystals take up the mobile atoms dissociated from the smaller crystals.[27] In addition, degradation of the MOF by electron beam during the TEM measurement plays a role in increasing the size of the MgH_2 crystal. Even after the formation of MgH_2, the organic ligands of SNU-90′ were not hydrogenated, as evidenced by the ^{1}H NMR spectra measured for the resulting nanocomposite that was dissolved in the mixture of DCl and $[D_6]Me_2SO$ (Supporting Information, Figure S3). When MgH_2@SNU-90′ was exposed to air, the PXRD pattern data showed new peaks at $2\theta = 36.8$ and 42.8 deg, which correspond to MgO, and a new peak at $2\theta = 38.0$ deg that corresponds to $Mg(OH)_2$, (Supporting Information, Figure S6).

In conclusion, we have prepared for the first time Mg nanocrystals in a MOF, and showed that Mg NCs@MOF is a hybrid-hydrogen-storage material that has both physical adsorption and chemisorption properties, and exhibits synergistic effects to increase isosteric heat of the H_2 physisorption and to decrease the temperatures for chemisorption/desorption of H_2. The present hybrid-hydrogen-storage material suggests a new strategy for H_2 storage and transport for the future. To develop the materials that are able to reach the DOE target, we are trying to further reduce the size of the Mg NCs and adjust the amount of loaded Mg in the selected physisorbed porous materials, such as light-weighted MOFs or organic COFs.[28] In addition, we are trying to develop new methods to protect the material from oxidation through air.

Received: July 28, 2012
Published online: September 7, 2012

Keywords: chemisorption · magnesium · metal–organic frameworks · nanocrystals · physisorption

[1] a) M. P. Suh, H. J. Park, T. K. Prasad, D.-W. Lim, *Chem. Rev.* **2012**, *112*, 782 – 835; b) J. Sculley, D. Yuan, H.-C. Zhou, *Energy Environ. Sci.* **2011**, *4*, 2721 – 2735; c) L. J. Murray, M. Dincă, J. R. Long, *Chem. Soc. Rev.* **2009**, *38*, 1294 – 1314.

[2] a) H. Furukawa, N. Ko, Y. B. Go, N. Aratani, S. B. Choi, E. Choi, A. Özgür Yazaydın, R. Q. Snurr, M. O'Keeffe, J. Kim, O. M. Yaghi, *Science* **2010**, *329*, 424 – 428; b) H. J. Park, D.-W. Lim, W. S. Yang, T.-R. Oh, M. P. Suh, *Chem. Eur. J.* **2011**, *17*, 7251 – 7260.

[3] Z. Wang, K. K. Tanabe, S. M. Cohen, *Chem. Eur. J.* **2010**, *16*, 212 – 217.

[4] Y.-G. Lee, H. R. Moon, Y. E. Cheon, M. P. Suh, *Angew. Chem.* **2008**, *120*, 7855 – 7859; *Angew. Chem. Int. Ed.* **2008**, *47*, 7741 – 7745.

[5] Y. E. Cheon, M. P. Suh, *Angew. Chem.* **2009**, *121*, 2943 – 2947; *Angew. Chem. Int. Ed.* **2009**, *48*, 2899 – 2903; *Angew. Chem.* **2009**, *121*, 2943 – 2947.

[6] E. Wiberg, H. Goeltzer, R. Bauer, *Z. Naturforsch. B* **1951**, *6*, 394 – 395.

[7] A. Zaluska, L. Zaluski, J. O. Strom-Olsen, *J. Alloys Compd.* **1999**, *288*, 217 – 225.

[8] L. Schlapbach, A. Züttel, *Nature* **2001**, *414*, 353 – 358.

[9] J.-L. Bobet, E. Grigorova, M. Khrussanova, M. Khristov, D. Radev, P. Peshev, *J. Alloys Compd.* **2002**, *345*, 280 – 285.

[10] V. Bérubé, G. Radtke, M. Dresselhaus, G. Chen, *Int. J. Energy Res.* **2007**, *31*, 637 – 663.

[11] K.-F. Aguey-Zinsou, J. R. A. Fernandez, T. Klassen, R. Bormann, *Int. J. Hydrogen Energy* **2007**, *32*, 2400 – 2407.

[12] W. Li, C. Li, H. Ma, J. Chen, *J. Am. Chem. Soc.* **2007**, *129*, 6710 – 6711.

[13] X. Zhang, R. Yang, J. Yang, W. Zhao, J. Zheng, W. Tian, X. Li, *Int. J. Hydrogen Energy* **2011**, *36*, 4967 – 4975.

[14] P. E. de Jongh, R. W. P. Wagemans, T. M. Eggenhuisen, B. S. Dauvillier, P. B. Radstake, J. D. Meeldijk, J. W. Geus, K. P. de Jong, *Chem. Mater.* **2007**, *19*, 6052 – 6057.

[15] I. Haas, A. Gedanken, *Chem. Commun.* **2008**, 1795 – 1797.

[16] K.-J. Jeon, H. R. Moon, A. M. Ruminski, B. Jiang, C. Kisielowski, R. Bardhan, J. J. Urban, *Nat. Mater.* **2011**, *10*, 286 – 290.

[17] a) H. R. Moon, J. H. Kim, M. P. Suh, *Angew. Chem.* **2005**, *117*, 1287 – 1291; *Angew. Chem. Int. Ed.* **2005**, *44*, 1261 – 1265; b) M. P. Suh, H. R. Moon, E. Y. Lee, S. Y. Jang, *J. Am. Chem. Soc.* **2006**, *128*, 4710 – 4718; c) Y. E. Cheon, M. P. Suh, *Chem. Eur. J.* **2008**, *14*, 3961 – 3967; d) H. R. Moon, J. H. Kim, M. P. Suh, *Eur. J. Inorg. Chem.* **2010**, 3795 – 3803.

[18] a) M. Meilikhov, K. Yusenko, D. Esken, S. Turner, G. V. Tendeloo, R. A. Fischer, *Eur. J. Inorg. Chem.* **2010**, 3701 – 3714; b) Y. K. Park, S. B. Choi, H. J. Nam, D. Y. Jung, H. C. Ahn, K. Choi, H. Furukawa, J. Kim, *Chem. Commun.* **2010**, *46*, 3086 – 3088.

[19] H. K. Chae, D. Y. Siberio-Pérez, J. Kim, Y. Go, M. Eddaoudi, A. J. Matzger, M. O'Keeffe, O. M. Yaghi, *Nature* **2004**, *427*, 523 – 527.

[20] A. P. Nelson, O. K. Farha, K. L. Mulfort, J. T. Hupp, *J. Am. Chem. Soc.* **2009**, *131*, 458 – 460.

[21] A. G. Turnbull, *Aust. J. Chem.* **1967**, *20*, 2059 – 2067.

[22] a) B. J. Kooi, G. Palasantzas, J. T. M. De Hosson, *Appl. Phys. Lett.* **2006**, *89*, 161914; b) C. Zhu, S. Hosokai, I. Matsumoto, T. Akiyama, *Cryst. Growth Des.* **2010**, *10*, 5123 – 5128.

[23] R. J. T. Houk, B. W. Jacobs, F. E. Gabaly, N. N. Chang, A. A. Talin, D. D. Graham, S. D. House, I. M. Robertson, M. D. Allendorf, *Nano Lett.* **2009**, *9*, 3413 – 3418.

[24] D. N. Mastronarde, *J. Struct. Biol.* **1997**, *120*, 343 – 352.

[25] B. Sakintuna, F. Lamari-Darkrim, M. Hirscher, *Int. J. Hydrogen Energy* **2007**, *32*, 1121 – 1140.

[26] C. Zlotea, J. Lu, Y. Andersson, *J. Alloys Compd.* **2006**, *426*, 357.

[27] M. Di Vece, D. Grandjean, M. J. Van Bael, C. P. Romero, X. Wang, S. Decoster, A. Vantomme, P. Lievens, *Phys. Rev. Lett.* **2008**, *100*, 236105.

[28] a) A. P. Côté, A. I. Benin, N. W. Ockwig, A. J. Matzger, M. O'Keeffe, O. M. Yaghi, *Science* **2005**, *310*, 1166 – 1170; b) K. Sumida, M. R. Hill, S. Horike, A. Dailly, J. R. Long, *J. Am. Chem. Soc.* **2009**, *131*, 15120 – 15121.

